RSC Advances

This is an *Accepted Manuscript*, which has been through the Royal Society of Chemistry peer review process and has been accepted for publication.

Accepted Manuscripts are published online shortly after acceptance, before technical editing, formatting and proof reading. Using this free service, authors can make their results available to the community, in citable form, before we publish the edited article. This *Accepted Manuscript* will be replaced by the edited, formatted and paginated article as soon as this is available.

You can find more information about *Accepted Manuscripts* in the Information for Authors.

Please note that technical editing may introduce minor changes to the text and/or graphics, which may alter content. The journal's standard Terms & Conditions and the Ethical guidelines still apply. In no event shall the Royal Society of Chemistry be held responsible for any errors or omissions in this *Accepted Manuscript* or any consequences arising from the use of any information it contains.

ROYAL SOCIETY OF CHEMISTRY

www.rsc.org/advances

RSC Advances

RSCPublishing

ARTICLE

Fire retardant mechanism of ethylene vinyl acetate elastomer (EVM) containing aluminium trihydroxide and melamine phosphate

Cite this: DOI: 10.1039/xoxxoooooox

Received ooth January 2012,
Accepted ooth January 2012

DOI: 10.1039/xoxxoooooox

www.rsc.org/

C. Hoffendahl,[a] G. Fontaine,[a] S. Duquesne,[a] F. Taschner,[b] M. Mezger,[b] S. Bourbigot[a]

Fire retardancy and smoke release of ethylene vinyl acetate (vinyl acetate content of 60 %, EVM) with aluminium trihydroxide (ATH) and melamine phosphate (MP) are evaluated by cone calorimetry, limiting oxygen index (LOI), UL-94 and a home-made smoke test. It was found that EVM-ATH has better fire retardant properties and lower smoke emission than the pure polymer. Partial substitution of ATH by MP led to further increase in LOI but earlier ignition of the material measured by cone calorimetry. Moreover, less smoke is released for EVM-ATH-MP than for EVM-ATH. Fire retardant mechanism was investigated for EVM-ATH and EVM-ATH-MP to evaluate the role of MP in the material. The dispersion of the additives was examined by scanning electron microscopy (SEM) showing that all additives are homogenously dispersed in the matrix. Further the thermal decomposition, the condensed and the gas phase mechanism of both materials was investigated using thermogravimetric analysis (TGA), mass loss calorimeter coupled with a Fourier transform infrared spectrometer (MLC-FTIR), pyrolysis-gas chromatography-mass spectrometry (py-GCMS), and solid state nuclear magnetic resonance (NMR) of ^{13}C, ^{27}Al and ^{31}P. It was shown that both materials are protected by a gas and condensed phase mechanism. The endothermic decomposition of ATH has a cooling effect and dilutes the fuel through release of water. In the condensed phase, it was found that both materials are protected through formation of a physical barrier. It is evidenced that the barrier formed for EVM-ATH-MP exhibits higher insulative properties than in the case for EVM-ATH.

1 Introduction

Polymers are quantitatively the most important products of the chemical industry used worldwide in everyday live. Polymers are used in medicine, in textiles, for packaging, in building industry etc. One of the main drawbacks of polymeric materials is their high flammability. Therefore, it is necessary to flame retard materials for many of the previously cited applications. In the last decade, it was already possible to decrease the total number of fire deaths thanks to concentrated use of fire retarded materials. The number of fire death was decreased in the USA from 4013 persons in 2001 to 3445 persons in 2010 [1]. In this paper fire retardancy of ethylene vinyl acetate with a vinyl acetate content of 60 % (EVM) is discussed. EVM has a huge range of applications: electronic devices, electrical engineering, wire and cables, buildings, transportation (aircraft, cars), photovoltaic etc. For many of these applications, it is required to fire retard EVM to meet the regulation. The most common method to enhance flammability properties of EVM based materials is the incorporation of mineral fillers, e.g. aluminium trihydroxide (ATH) or magnesium dihydroxide (MDH) [2]. However, high loadings of this type of filler (higher than 50 wt%) are required to enhance fire retardancy of EVM leading to dramatically change of the mechanical properties of the material [3, 4]. To overcome this disadvantage, mineral fillers can be incorporated in combination with other conventional flame retardants. In literature, mineral fillers are often combined with phosphorous compounds [5-7], nitrogen containing additives [8], silicone compounds [9, 10] or nanoadditives [11-16] to improve fire retardant properties and to decrease smoke release in some cases. Zilberman et al. [8] showed that the incorporation of ATH in combination with melamine enhances the fire retardant properties of ethylene vinyl acetate but also increases the smoke release in comparison to the pure polymer. To overcome an increase in the smoke production maintaining the improved fire retardant properties, ATH will be combined with melamine phosphate (MP) in this study. As far as we know, up to now nothing is reported in literature about the combination of ATH and MP in EVM-materials.

In the first part of this paper fire retardancy and smoke release of EVM-materials containing ATH and MP will be investigated.

RSC Advances Accepted Manuscript

Afterwards the dispersion of the additives in the polymeric matrix will be analysed via scanning electron microscopy (SEM). The decomposition mechanism of EVM-materials containing ATH in combination with MP will be finally investigated using thermogravimetric analysis (TGA), solid state nuclear magnetic resonance (NMR) (^{13}C, ^{27}Al and ^{31}P), pyrolysis-gas chromatography-mass spectrometry (py-GSMS) and mass loss calorimeter coupled with a Fourier transform infrared spectrometer (MLC-FTIR).

2 Experimental

2.1 Materials

Levapren®600 (hereafter called EVM), an ethylene-vinyl acetate with 60 wt% vinyl acetate, was supplied by LANXESS. Aluminium trihydroxide (hereafter called ATH) was supplied in powder from Nabaltec as Apyral 120E (BET = 11 m²/g). Melagard MP, melamine phosphate (hereafter called MP) was received in powder from Italmatch Chemicals. Rhenofit TAC/S (triallyl cyanurate) was supplied by LANXESS in powder. Perkadox 14-40B-PD (Bis(tert-butyldioxyisopropyl) was received from Akzo Nobel in powder.

2.2 Processing of materials

Samples were prepared following an upside down process in an internal mixer GK 1.5L from Werner & Pfleiderer. Mixing was performed at 20 °C with a rotation speed of 40 rpm for 4 min. Additives were added into the mixing chamber before the polymer. After mixing, materials were further dispersed on an open two roll mill at 20 °C. Vulcanization agents, Perkadox TAC/s (6 phr) and Rhenofit (1 phr), were added afterwards on the two roll mill. After batch off and 24h relaxation time, materials were treated a second time with the two roll mill. Later the compounds were pressed into plates and vulcanized at 180 °C for 12 min. Composition and name of the prepared formulations are gathered in Table 1.

Table 1: Composition and name of the formulations EVM/ATH/MP

Formulation Name	EVM [phr]	FR [phr]	ATH [phr]	MP [phr]
EVM	100	0	0	0
EVM-ATH	100	130	130	0
EVM-ATH-MP	100	130	108	22

2.3 Fire testing

Fire Testing Technology (FTT) Mass Loss Calorimeter was used to perform measurements on samples following the procedure defined according to ASTM E 906. The equipment is identical to that used in oxygen consumption cone calorimetry (ASTM E-1354-90), except that a thermopile in the chimney is used to obtain heat release rate (HRR) rather than employing the oxygen consumption principle. Our procedure involved exposing plates (100 x 100 x 3 mm³) in horizontal orientation. Samples are covered by a grid to prevent swelling. Samples were then wrapped in aluminium foil leaving the upper surface exposed to the heater (external heat flux = 35 kW/m²) and placed on a ceramic backing board at a distance of 25 mm from cone base. The mass loss calorimeter is used to determine the following principal fire properties: heat release rate (HRR) as a function of time, time to ignition (TTI) and total heat release (THR). When measured at 35 kW/m², HRR, THR and TTI values are reproducible to within ±10%.

To investigate the gases released during MLC experiment, MLC was connected to a Fourier transform infra-red spectrometer (MLC-FTIR). Using this device released gases are analysed online quantitatively and qualitatively. Gas picking pistol and transfer line were provided by M&C Tech Group; FTIR, Antaris™ Industrial Gas System, was provided by ThermoFisher. The transfer line between MLC and FTIR is 2 m long and was heated up to 200 °C. To assure constant temperature of the transfer line, two temperature controllers were installed. Before analysing the gases by FTIR, soot particles were filtered off by two different heated filters (2 and 0.1 µm). Filters consist of glass fibres and ceramic respectively. The FTIR gas cell was set to 185 °C and 652 Torr. The optical pathway is 2 m long and the chamber of the spectrometer is filled with dry air. FTIR spectra obtained using MLC-FTIR were treated using OMNIC software. To quantify gases, spectra have to be recorded at different concentrations for targeted gases and a quantification method has to be created using TQ Analyst. To create a method, representative regions in the spectra of the selected gas have to be chosen and interactions with other gases have to be taken into account. Using MLC-FTIR the following gases can be quantified: water, carbon monoxide, carbon dioxide, acetic acid, ammonia, methane, nitrogen monoxide, nitrogen dioxide, hydrogen cyanide. Quantification is reproducible within ± 10%.

Limiting Oxygen Index (LOI = minimum oxygen concentration to support candle-like combustion of plastics) was measured using a Fire Testing Technology (FTT) instrument on sheets (100 x 10 x 3 mm^3) according to the standard 'oxygen index' test (ISO4589). It measures the minimum concentration of oxygen in a nitrogen/oxygen mixture required to just support combustion of a test sample under specified test conditions in a vertical position (the top of the test sample is ignited with a burner).

UL-94 tests were performed according to IEC 60695-11-10 on samples 127 x 13 x 15 mm³. It describes the tendency of a material to extinguish or to spread the flame after ignition of the material. It classifies specimens from V-0, V-1 to V-2, where V-0 is the best rating.

2.4 Smoke opacity test

Smoke opacity test used in this study is a homemade test developed to evaluate the smoke release during combustion (Fig. 1). The structure is similar to that of the mass loss calorimeter. An external heat flux of 35 kW/m² produced by a conical heater was applied on a horizontal sample (100 x 100 x 3 mm³). The distance between the heating element and the sample was fixed at 35 mm (instead of 25 mm for MLC) which

RSC Advances Accepted Manuscript

 This journal is © The Royal Society of Chemistry 2014

permits to work without grid on the sample surface. Samples were ignited by a spark igniter. The generated smoke was measured at the top of the chimney with a smoke density analyser TRDA 302 from Taurus Instrument. A light source (halogen point light source) emits light (intensity I_0) and the transmitted light (intensity I) was measured by a light sensor. Curves of optical density (OD = -log I/I_0) versus time present smoke release during combustion. The following values were determined using smoke opacity test: total optical density (OD_{total}), VOF4, i.e. the summation of the optical density (OD) over the first four minutes, maximum optical density during the experiment (D_s1 for the first local maximum and D_s2 for the second local maximum of the curve) and the maximum optical density during the first four minutes (D_s4).

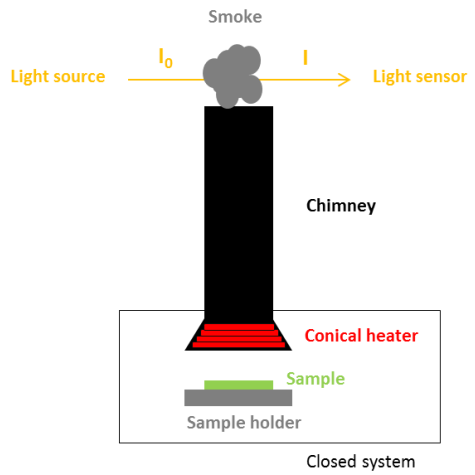

Fig. 1: Schematic presentation of smoke test device

2.5 Microscopy

Scanning electron microscopy (SEM) images were taken at various levels of magnification using a Hitachi S4700 SEM at 6 kV. All samples were ultra microtomed with a diamond knife on a Leica UltraCut microtome at cryo temperature (−120◦C) to obtain smooth surfaces.

2.6 Thermal analysis

Thermogravimetric analysis was carried out on a TA Instrument (TGA Q5000IR). The balance purge flow was set to 15 mL/min and the sample purge flow (nitrogen) to 100 mL/min. The powdered samples put in open alumina pan underwent a heating from 50 to 800 °C with a heating rate of 10 °C/min.

2.7 Pyrolysis GCMS (py-GCMS)

Pyrolysis-Gas chromatography-mass spectrometry (py-GCMS) analyses were performed on a device provided by Shimadzu. The device consists of a micro-furnace pyrolyzer (Frontier Lab PY-2020iD) coupled with a GCMS device (Shimadzu GCMS QP2010 SE). Experiments are performed under inert conditions using helium. Sample size is about 200 µg. Tests were performed using the desorption mode, i.e. the samples (in a stainless steel cup) are heated up in the furnace to the desired temperature with a chosen heating rate (10 °C/min or infinite). This heating rate was chosen to mimic the TGA-FTIR experiment and to get more information about gases evolved during pyrolytic decomposition. After the desorption process, evolved gases were introduced into the GCMS system whereas a part of the gases was split to avoid blockage in the column or saturation of the detector. Released decomposition gases were separated using a 30 m long fused silica capillary column. The temperature of the column was set at 35 °C during the desorption process. The column was then heated up to 300 °C with a heating rate of 10 °C/min followed by an isotherm at 300 °C for 30 min. The linear velocity of the carrier gas (helium) was set at 40 cm/s. The separated gases and fragments were then analysed with the quadrupole mass spectrometer with an Electron-Impact (IE) ionization source. The IE spectra were recorded at 70 eV with a mass scan of 2 scans per second. The interface between the pyrolyzer and the GC was heated up to 320 °C; the interface GC-MS to 280 °C. The ion source had a temperature of 230 °C. Obtained chromatograms were treated using F-Search (Frontier Lab) whereas NIST mass spectral database was used for identification of molecules.

2.8 Solid State NMR

^{13}C solid state NMR spectra were recorded at 100.6 MHz (B_0 = 9.4 T) on Bruker Avance II 400 using a 4 mm standard probe. The conditions were cross-polarization (CP) ^{1}H-^{13}C (contact time of 1 ms) with dipolar decoupling (DD) and magic angle spinning (MAS) at 10 kHz. The recycle delay between two pulses was 5 s. The number of scans was 1024 and ^{13}C chemical shifts were referenced to tetramethylsilane (TMS).
^{27}Al NMR measurements were carried out at a frequency of 24.5 MHz on a Bruker Avance II 400 (B_0 = 9.4 T) with a probe head of 4 mm using MAS at 12.5 kHz. The repetition time was fixed at 1 s for all samples. The number of scans was fixed to 128. The reference used was 1 M solution of aluminium nitrate.
^{31}P NMR measurements were obtained at a frequency of 40.1 MHz on a Bruker Avance II 400 (B_0 = 9.4 T) with a probe head of 4 mm using MAS at 12.5 kHz. Phosphoric acid was used as reference. Number of scans was set to 16 and repetition time was fixed at 120 s to ensure complete signal relaxation.

3 Results and discussion

3.1 Microscopy

The dispersion of ATH and MP in EVM-ATH and EVM-ATH-MP was examined using SEM. Fig. 2 (a) shows a SEM image of the ATH particles in EVM-ATH. ATH particles are well dispersed in the polymeric matrix exhibiting a size lying between 0.5 and 1 µm. This consists with data indicated by the supplier for the particle size of ATH
Dispersion of ATH and MP particles in EVM-ATH-MP is presented in Fig. 2 (b, c). The dispersion of ATH in EVM-ATH-MP is similar to that observed for EVM-ATH.

RSC Advances Accepted Manuscript

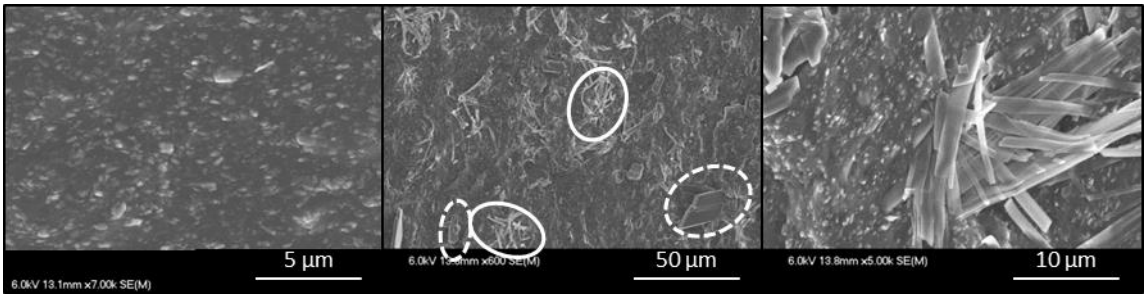

Fig. 2: SEM image EVM-ATH (a) and EVM-ATH-MP (b,c)

In the case of MP particles two different types of agglomerates are observed: agglomerates formed with needle-like particles (circled straight line) and particle agglomerates (circled dotted line). Both sorts of agglomerates are due to the presence of MP in the polymeric matrix. The crystal-like agglomerates have a size of around 16 to 33 µm, whereas it is possible that they are even bigger due to the fact that only a cross-section of the material is presented. In the case of the agglomerates consisting of needle-like structures, the size of single needles is up to 20 µm, whereas their thickness/diameter varies between 0.1 and 0.5 µm.

3.2 Fire retardancy and smoke release

Fig. 3 shows HRR curves for the tested materials. The corresponding values, i.e. peak of heat release rate (pHRR), reduction in pHRR in comparison to the pure polymer, THR, TTI and the mass loss during combustion as well as the LOI values and UL-94 classification of the tested materials are presented in Table 2.

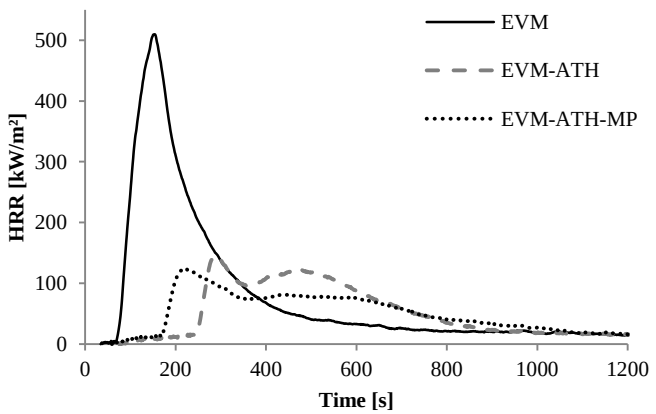

Fig. 3: Heat release rate (HRR) curves at 35 kW/m2

The virgin polymer has a pHRR of 510 kW/m², a THR of 97 MJ/m², a TTI of 67 s. After the combustion nearly no material remains in the aluminium foil. Incorporation of 130 phr of ATH leads to a decrease of pHRR by 71 % in comparison to the virgin polymer (146 kW/m²) and a THR of 60 MJ/m² which corresponds to a reduction of 38 % in comparison to the pure polymer. EVM-ATH has a mass loss of 61 % and a TTI of 245 s. Partial substitution of ATH by MP (ratio 5:1, EVM-ATH-MP) leads to comparable pHRR (124 kW/m²), THR (60 MJ/m²) and ML (64 %) as it is observed for the material containing only ATH (EVM-ATH). It is noteworthy that in the case of EVM-ATH-MP, $pHHR_2$ (78 kW/m²) is significantly smaller than that of EVM-ATH (123 kW/m²). EVM-ATH-MP has a TTI of 167 s which is increased in comparison to the pure polymer but decreased in comparison to EVM-ATH.

The LOI value increases from 19 vol%O_2 for the pure polymer to a value of 33 vol%O_2 for EVM-ATH and to 38 vol%O_2 in the case of EVM-ATH-MP. Both materials, EVM-ATH and EVM-ATH-MP reach V-0 classification in UL-94 test, whereas the pure polymer is non-classified.

Optical density curves measured during combustion of the tested materials and corresponding values are presented in Fig. 4 and Table 2.

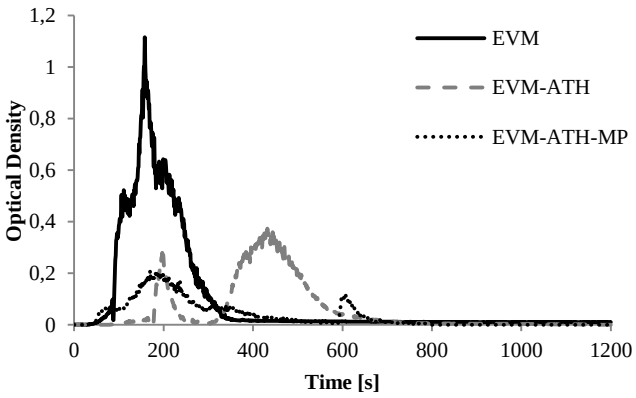

Fig. 4: Optical density (OD) curves at 35 kW/m^2 of EVM-ATH-MP formulations

The pure polymer, EVM, has an OD_{total} of 114, a VOF4 value of 87 and a D_S4 as well as D_S1 of 1.1. Incorporation of 130 phr of ATH leads to a decrease of smoke release. OD_{total} of EVM-ATH is decreased to a value of 67 and VOF4 is decreased to 9. EVM-ATH has further a D_s4 and D_s1 of 0.3 and a D_s2 value of 0.4. Combination of ATH and MP in EVM (EVM-ATH-MP) further reduces the total optical density observed during the experiment. EVM-ATH-MP has an OD_{total} value of 48, which corresponds to a decrease by 60 % in comparison to the pure polymer. D_s4 and D_s1 are 0.2; D_s2 is 0.1. D_s2 peak in the smoke curved of EVM-ATH-MP is due to extinguishment of the material. D_s values are all decreased in comparison to EVM and EVM-ATH.

RSC Advances Accepted Manuscript

Table 2: Fire retardant properties and smoke release of EVM, EVM-ATH and EVM-ATH-MP

Material	pHRR [kW/m²]	pHRR reduction [%]	THR [MJ/m²]	THR reduction [%]	TTI [s]	ML [%]	LOI [vol%O_2]	UL-94	OD_{total}	VOF 4	D_s4	D_s1	D_s2
EVM	510	-	97	-	67	96	19	NC	114	87	1.1	1.1	-
EVM-ATH	146	71	60	38	245	61	33	V-0	67	9	0.3	0.3	0.4
EVM-ATH-MP	124	76	60	38	167	64	38	V-0	48	23	0.2	0.2	0.1

Regarding VOF4 it appears that EVM-ATH-MP has a value of 23 which corresponds to an increase in comparison to EVM-ATH but a significant decrease in comparison to the virgin polymer. The high VOF4 value is explained by the fact that EVM-ATH-MP releases smoke during the first 400 s whereas nearly no smoke is evolved from 400 to 1200s. For EVM-ATH more smoke is evolved from 400 to 1200 s than from 0 to 400 s.

3.3 Decomposition mechanism

The decomposition mechanism of EVM-ATH and EVM-ATH-MP is investigated in the following part. First thermal decomposition of the additives and of the materials are discussed. Then, the gas and condensed phase for both materials are analysed.

3.3.1 Thermal analysis

TG curves in nitrogen and air of individual compounds, i.e. EVM, ATH and MP are presented in Fig. 5. The decomposition of EVM is already reported in literature [17]. The pyrolytic decomposition of EVM shows three steps. The first step occurs between 250 and 390 °C (T_{max} = 350 °C, 42 wt% mass loss). This step corresponds to the deacetylation of the polymer. During this step acetic acid is evolved and the polymer is decomposed into linear polyenes. The second step is observed between 390 and 510 °C (T_{max} = 470 °C, 54 wt% mass loss) and is attributed to the decomposition of the polyenes that were formed before. The third step occurs between 600 and 680 °C (T_{max} = 650 °C) with a mass loss of 1 wt%. This step is due to the presence of Perkadox (Bis(tert-butyldioxyisopropyl) benzene) which is used for vulcanization of the material. At the end of the pyrolytic decomposition of EVM a residue of 2wt% is left. The thermo-oxidative decomposition of the EVM is more complex than that under inert conditions; it is a five step process. The first one occurs from 200 to 220 °C (1 wt% mass loss), the second one is observed between 220 and 410 °C (T_{max} = 335 °C, 56 wt% mass loss), the third one from 410 to 480 °C (T_{max} = 445 °C, 23 wt% mass loss), the fourth one from 480 to 570 °C (T_{max} = 510 °C, 16 wt% mass loss) and the fifth step occurs between 570 and 670 °C (T_{max} = 645 °C, 1 wt% mass loss). At the end of the thermo-oxidative decomposition a residue of 2.5 wt % is left. Concerning the thermal decomposition of ATH it can be seen that the thermo-oxidative as well as the pyrolytic decomposition of ATH are similar. It has two steps, one between 160 and 200 °C (mass loss 1 wt%) and the second one from 200 to 315 °C (T_{max} = 270 °C, mass loss 30 wt%). The first small step can be attributed to the partial decomposition of gibbsite ($Al(OH)_3$) into boehmite (AlO(OH)) [18]. The second step between 200 and 315 °C is due to the complete dehydration of the hydroxide into oxide (Al_2O_3) [2]. At the end of the pyrolytic as well as the thermo-oxidative decomposition a residue of 63 wt% is left. The data found for decomposition of MP, corresponds to that already reported in literature[19-22]. It can be seen that MP has a comparable thermal decomposition in air and nitrogen. The first step occurs from 200 to 285 °C (T_{max} = 275 °C, 5 wt% mass loss) and the second one from 285 to 330 °C (T_{max} = 310 °C, 5 wt% mass loss). These two steps are attributed to dehydration processes. In the first step melamine phosphate condensates to melamine pyrophosphate which is transformed into melamine polyphosphate in the second dehydration step. The third step takes place from 330 to 420 °C (T_{max} = 390 °C, 13 wt% mass loss). During this step the melamine polyphosphate degrades to melam ultraphosphate evolving water, ammonia and melamine. The fourth step takes place from 420 to 530 °C (5 wt% mass loss). The fifth step differs depending on the conditions. In air the fifth decomposition step occurs from 530 to 690 °C (T_{max} = 560 °C, 27 wt% mass loss); in nitrogen from 530 to 705 °C (T_{max} = 560 °C, 21 wt% mass loss). From 420 to around 700 °C the melam ultraphosphate is degraded leaving a residual mass of 25 (in air) and 29 wt % (in nitrogen) respectively.

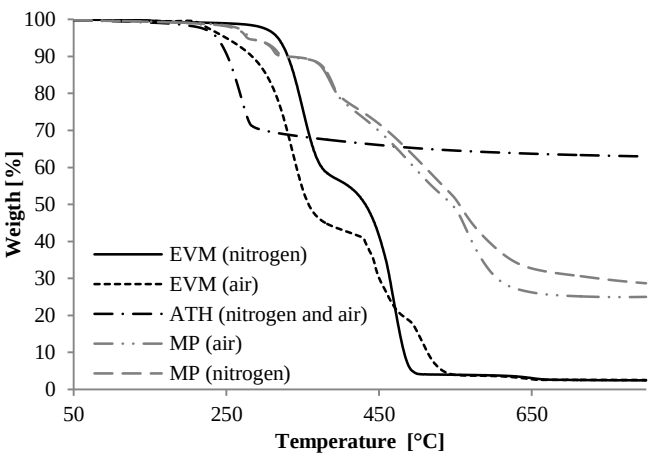

Fig. 5: TG curves of EVM-ATH and EVM-ATH-MB (10°C/min, under nitrogen and air)

RSC Advances Accepted Manuscript

TG curves of the materials, EVM-ATH and EVM-ATH-MP are presented in Fig. 6. Thermal decomposition of ethylene vinyl acetate materials containing ATH is already reported in literature [23]. Therefore the observed decomposition steps in pyrolytic and thermo-oxidative conditions for EVM-ATH can be discussed in details. Pyrolytic decomposition of EVM-ATH is a four step process. The first step occurs from 180 to 315 °C (T_{max} = 265 °C). The weight loss during this step is 17 wt% which corresponds to the mass lost during dehydration of ATH. The second step is obtained from 315 to 400 °C (T_{max} = 350 °C, 16 % weight loss). This step can be attributed to the deacetylation reaction of EVM. The third pyrolytic decomposition step takes place from 400 to 540 °C with a mass loss of 27 wt% (T_{max} = 470 °C). This step can be attributed to the decomposition of the polyenes that were formed during the deacetylation of the polymer. This could be due to the formation of a char residue which results in a less important mass loss. The last decomposition step occurs from 625 up to 700 °C with a maximum weight loss at 660 °C and a weight loss of 1 wt%. This step can be attributed to the presence of vulcanization agents in the material and its decomposition. At the end of the pyrolytic decomposition a residue of 37 wt% is left. In the case of the thermo-oxidative decomposition of EVM-ATH (100-130) a five-step-process is obtained. The first decomposition under thermo-oxidative conditions is similar to that of the pyrolytic decomposition, it takes place from 180 to 315 °C (T_{max} = 290 °C, 21 % weight loss) and is attributed to the decomposition of ATH. During the second step (315 – 410 °C, T_{max} = 335 °C) a mass loss of 18 wt% is observed. The third decomposition step occurs from 410 to 480 °C (T_{max} = 450 °C) with a corresponding mass loss of 15 wt%. From 480 to 580 °C a fourth step takes place (T_{max} = 500 °C, 9 % weight loss). The last step in thermo-oxidative conditions occurs between 580 and 675 °C. A residue of 35 wt% is left at the end of the decomposition process.

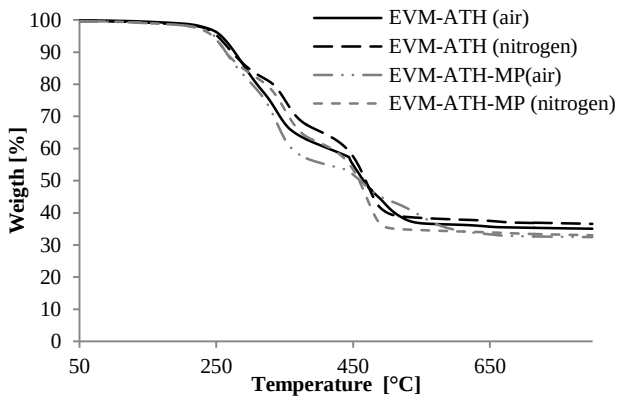

Fig. 6: TG curves of EVM-ATH and EVM-ATH-MP (10°C/min, under nitrogen and air)

In contrast to the thermal decomposition of EVM-ATH, the decomposition of EVM-ATH-MP is not reported in literature. The pyrolytic decomposition of EVM-ATH-MP is a three-step process. The first step of EVM-ATH-MP occurs from 180 to 305 °C (T_{max} = 250 °C, 16 % weight loss), the second one from 305 to 390 °C (T_{max} = 350 °C, 20 % weight loss) and the third one from 390 to 520 °C (T_{max} = 470 °C, 27 % weight loss). At the end of the pyrolytic decomposition process a residue of 33 wt% is left. The thermo-oxidative decomposition of EVM-ATH-MP takes places in five steps. The first one takes place from 180 to 300 °C (T_{max} = 260 °C, 18 % weight loss), the second one from 300 to 430 (T_{max} = 340 °C, 27 % weight loss), the third one from 430 to 500 °C (T_{max} = 450 °C, 10 % weight loss), the fourth one from 500 to 640 °C (T_{max} = 540 °C, 10 % weight loss) and the fifth one from 640 to 700 °C (T_{max} = 660 °C, 1 % weight loss). The third step has two local maxima whereas the highest decomposition rate is obtained at 540 °C. At the end of the thermo-oxidative decomposition of EVM-ATH-MP (100-108-22) a residue of 33 wt% is left.

3.3.2 Gas phase analysis

In this part, gases released during decomposition of EVM-ATH and EVM-ATH-MP are analysed. Investigation of gases released during decomposition of EVM-ATH is already reported in literature [23]. In this study, gases are analysed using simultaneous thermal analysis with evolved gas analysis (STA-FTIR). To go further in the comprehension of gas phase, two other methods are used in our study: py-GCMS and MLC-FTIR. First gases released during pyrolytic decomposition of EVM-ATH and EVM-ATH-MP are detected using py-GCMS. This method is based on thermal decomposition investigated by TGA; released gases are analysed after each decomposition step. Then decomposition in thermo-oxidative conditions is further investigated using MLC-FTIR. Released gases are detected quantitatively during experiment.

EVM-ATH

Fig. 7 presents the chromatograms obtained by py-GCMS in inert conditions for EVM-ATH. First of all, it has to be mentioned that the peak (air) present in the mass spectra corresponds to air that is left in the interfaces and which is evolved into the column after heating ramp of the material. From 50 to 315 °C, the following gases are detected: water (1) coming from the decomposition of ATH, acetic acid (2) evolved during deacetylation of the polymer and different molecules (3) due to the presence of vulcanization agents in the material. The chromatogram between 315 and 400 °C shows the presence of hydrocarbons (5), whereas saturated and monounsaturated hydrocarbon structures from C8 to C34 are found. Moreover, a big peak at early retention times is detected (4). This peak can be attributed to the presence of acetic acid and acetone. The formation of acetone is explained through transformation of acetic acid into acetone. This reaction is possible due to the presence of alumina formed by decomposition of ATH in the condensed phase, which has a catalytic effect on the formation reaction of acetone [23, 24]. These latter studies reported that during decomposition of the EVA-ATH materials no acetic acid was detected in the gas phase; instead acetone was found. However, these studies were performed on EVA-materials having low VA contents. The content of VA in this study is more than two times higher than in the studies reported in literature. It is supposed that the high

RSC Advances Accepted Manuscript

 This journal is © The Royal Society of Chemistry 2014

quantity of VA and therefore the resulting high quantity of acetic acid released during decomposition lead to the fact that not all acetic acid molecules are transformed into acetone by catalytic reaction through alumina. Moreover, conditions used in this study are different: Witkowski et al. [23] analysed gases evolved during decomposition using simultaneous thermal analysis with evolved gas analysis (STA-FTIR) with controlled heating ramp.

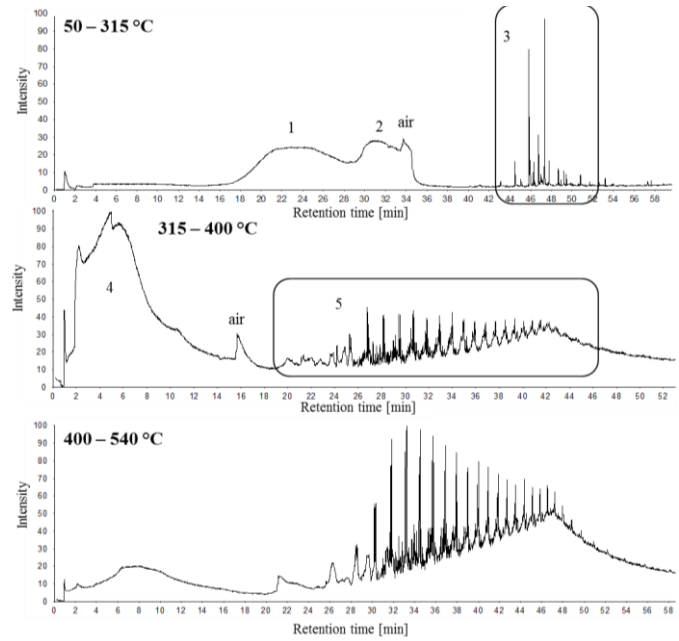

Fig. 7: Chromatograms of EVM-ATH, 10°C/min

Regarding gases present in the gas phase from 315 to 400 °C it can be said that in this temperature range the deacetylation of the polymer is complete. Moreover, polyenes formed during deacetylation also start to degrade in this temperature range.

From 400 to 540 °C, peaks indicating the presence of hydrocarbon structures are found. The structures of the hydrocarbons are equal to those obtained before, from 315 to 400 °C. In this temperature range the decomposition of polyenes formed during deacetylation of the polymer takes place. Between 540 and 800 °C peaks corresponding to Perkadox (Bis(tert-butyldioxyisopropyl) benzene), a vulcanization agent, are detected. Moreover, unsaturated hydrocarbons containing 18 to 49 carbon atoms are found. Looking at the analysis of the gas phase in inert conditions (low heating ramp) using py-GCMS, it can be said that EVM-ATH is first protected by dilution of the fuel. Fuel is diluted through water coming from the endothermic decomposition of ATH. During the first decomposition step of EVM-ATH the deacetylation of the polymer forming a polyene residue takes place. The formed polyenes start to degrade during deacetylation and are fully degraded afterwards.

Changing the heating ramp from 10 °C/min to an infinite heating ramp, the decomposition gases change completely. Fig. 8 presents the chromatogram obtained at infinite heating ramp. This process leads to detection of the following molecules: water (1), butadiene (2), acetone (3), cyclopentadiene (4), cyclopentene (5), 1-hexene (6), acetic acid (7), benzene (8), 1,3-cyclohexadiene (9), toluene (10), ethylbenzene (11), xylene (12), styrene (13), 1,8-nonadiene (13), 1-nonene (13), isopropylbenzene (14), ethyltoluene (14), 1-decene (14), methylstyrene (14), 1-propenylbenzene (15), indane (15), indene (16), 1-methylindene (17), ethylstyrene (17), 1-undecene (17), tetrahydronaphthalene (18), naphthalene (19), 1-methylnaphthalene (20), 2-methylnaphthalene (21), 3,3-dimethyl-1-indanone (22).

Thus, this indicates that decomposition of ATH evolves water like it is the case for low heating ramps. Concerning the polymer decomposition, deacetylation takes place like at low heating ramp – acetic acid and acetone are evolved. However, decomposition of the polyene structure formed during deacetylation is different for high heating ramps. Instead of saturated and monounsaturated hydrocarbons in the case of low heating ramps, benzene and its homologues are formed. It is assumed that at high heating rates, formation of benzene and its homologues is thermodynamically favoured over formation of linear hydrocarbons.

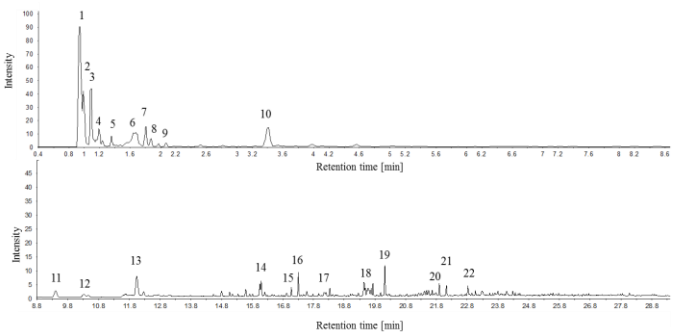

Fig. 8: Chromatogram of EVM-ATH, heating ramp infinite

The gas phase in thermo-oxidative conditions was analysed using MLC-FTIR. MLC-FTIR is a powerful tool to understand reactions going on during MLC experiment. Evolution of gases as a function of time is detected directly during experiment (Fig. 9).

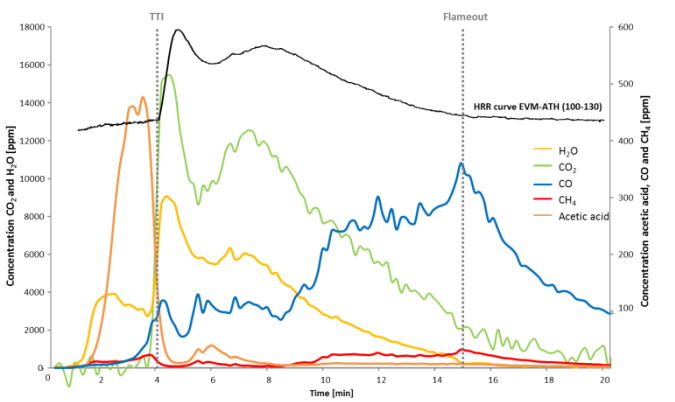

Fig. 9: Spectra obtained by MLC-FTIR for EVM-ATH

RSC Advances Accepted Manuscript

Before ignition of the material three main gases are released: acetic acid, water and methane. Before ignition 3796 ppm of acetic acid are detected; this corresponds to 73 % of total release. This indicates that deacetylation of the polymer is almost completed before ignition of EVM-ATH. Moreover it can be seen that release of acetic acid decreases already before ignition. Decrease of the concentration of acetic acid is therefore not due to ignition. This observation supports the assumption that deacetylation process is almost complete before ignition. Late ignition of the material, despite presence of flammable acetic acid, is explained by the presence of water (released during ATH decomposition) diluting the fuel. Moreover a small quantity of methane (186 ppm, 12% of total release) is also detected in the gas phase before ignition. The presence (or absence) of acetone in the gas phase cannot be confirmed regarding FTIR spectra.

Table 3: Quantification of released gases during MLC-FTIR experiment for EVM-ATH

Gas	Total quantity released [ppm]	Released before ignition [ppm]	Released before ignition [%]
H2O	303888	46229	15
CO2	592951	12257	2
CO	18368	208	1
CH4	1581	186	12
Acetic acid	5194	3796	73

Once the material starts to burn, a rapid increase of the concentration of carbon dioxide and water is observed. Carbon dioxide reaches a maximum concentration of 15432 ppm and water of 9045 ppm after ignition whereas concentration decreases afterwards. The presence of these two gases indicates complete combustion of the material. Besides carbon dioxide and water, carbon monoxide is detected in low quantity (100 ppm) indicating that also incomplete combustion is taking place but it has to be noted that complete combustion dominates the incomplete one. In the ongoing combustion process the quantity of methane released is comparable; the quantity never exceeds 50 ppm. At around 360 s an additional increase of concentration of carbon dioxide and water is found. Moreover, the concentration of acetic acid increases as well. At the same time, the HRR increases. Due to increase of quantity of gases in the gas phase between $pHRR_1$ and $pHRR_2$, it is supposed that a protective layer is formed on the material surface after ignition which is broken at around 360 s. This leads to a more important release of fuel into the flame and a therefore results in an increase of water and carbon dioxide in the gas phase. Until flameout and end of the combustion the concentration of carbon dioxide and water decreases constantly. In the case of carbon monoxide, the concentration increases up to 360 ppm until flameout at around 900 s. After flameout, concentration of carbon monoxide decreases. The same phenomenon is obtained for methane: after flameout the concentration decreases slightly. Over the whole experiment complete combustion dominates incomplete one whereas incomplete one is getting more important at the end of combustion. It is known that incomplete combustion leads to increased production of soot particles. The increased production of smoke in the second part of the combustion process in MLC experiment can therefore be explained by this fact.

The analysis of the gas phase action of EVM-ATH by py-GCMS and MLC-FTIR showed that the material is first protected through the presence of ATH in the material. ATH decomposes endothermically releasing water which dilutes the fuel. The polymer starts to degrade at the same time. First the deacetylation takes place. During this step a polyene network is formed which is then degraded evolving hydrocarbons. Structure of hydrocarbons depends on the chosen heating rate: low heating rates lead to saturated and mono unsaturated linear hydrocarbons, whereas high heating ramps lead mainly to formation of benzene and its homologues.

EVM-ATH-MP

Analysis of the gas phase under inert conditions (py-GCMS) of EVM-ATH-MP (Fig. 10) showed that up to 180 °C gases due to the presence of vulcanization agents (1) in the material are observed. Moreover, a small quantity of melamine (2) coming from the melamine phosphate was detected. Between 180 and 305 °C, water (3), melamine (5) and acetic acid (4) are detected in the gas phase. Additionally to these peaks, molecules due to the presence of the vulcanization agents are still detected (6). The presence of water indicates the decomposition of ATH into alumina, which is known to take place in this temperature range [2]. The presence of melamine proves the decomposition of MP. Moreover, it can be assumed that the deacetylation of the polymer starts in this temperature range (presence of acetic acid).

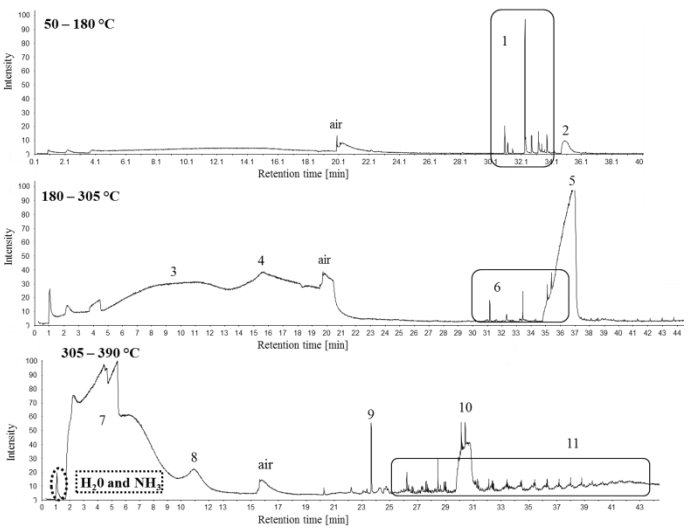

Fig. 10: Chromatograms of EVM-ATH-MP, 10°C/min

Between 305 and 390 °C, peaks corresponding to acetic acid (7), acetone (8), 3,5,5-trimethylcyclohex-2-enone (9) and melamine (10) are detected. Additionally peaks corresponding to saturated and monounsaturated hydrocarbons from C8 to C34 (11) are detected. As in the case of EVM-ATH, the presence of acetone is explained by the catalytic effect of alumina in the condensed phase. The presence of melamine

RSC Advances Accepted Manuscript

 This journal is © The Royal Society of Chemistry 2014

corresponds to thermal decomposition of MP as reported in literature [22]. In this temperature range, melamine phosphate degrades to melam ultraphosphate evolving water, ammonia and melamine. The peak corresponding to ammonia and water is also detected. From 390 to 520 °C and from 520 to 800 °C, gases detected in the gas phase of EVM-ATH-MP are similar to those obtained for EVM-ATH from 400 to 540 °C and from 540 to 800°C. Molecules containing phosphorous were not detected. It is therefore assumed that phosphorus acts in the condensed phase (it will be discussed in the following).

Gases evolved during pyrolytic decomposition of EVM-ATH-MP at high heating rate change completely compared to those obtained at low heating rate (Fig. 11). Chemical nature of released gases evolved from EVM-ATH-MP are similar to those obtained for EVM-ATH at high heating rate except of one peak that can be assigned to hydrogen isocyanate and isocyanic acid. Due to the fact that these gases are not detected for EVM-ATH it is assumed that their presence is due to MP in the material, whereas these gases were not detected during decomposition of EVM-ATH-MP at low heating ramps. As for the decomposition at low heating rate, molecules containing phosphorous are not detected in the gas phase.

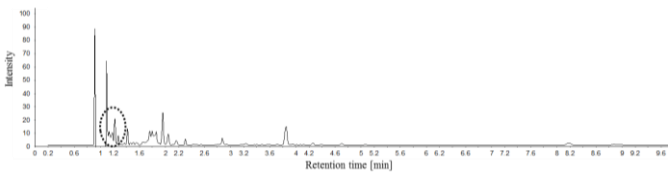

Fig. 11: Chromatogram of EVM-ATH-MP, heating ramp infinite

As for EVM-ATH, the gas phase in thermo-oxidative conditions for EVM-ATH-MP was analysed using MLC-FTIR (Fig 12).

Before ignition of the material, mainly water (17830 ppm), acetic acid (1738 ppm) and ammonia (867 ppm) are evolved whereas concentration of ammonia and acetic acid increase constantly until ignition of the material. As it was discussed for EVM-ATH, the presence of acetic acid indicates deacetylation of the polymer and presence of water proves that decomposition of ATH is taking place. Presence of ammonia in the gas phase is due to decomposition of MP [22]. Before, it was shown that EVM-ATH-MP ignites 78 s earlier than EVM-ATH. The earlier ignition can be explained through the presence of ammonia in the gas phase. Due to presence of ammonia and acetic acid more flammable gases are present in the gas phase than it is the case for the material without MP. At room temperature ammonia is known to ignite at 630 °C whereas its flammability range lies between 15 and 28 % in air. At the same time the amount of ATH in EVM-ATH-MP is smaller than in EVM-ATH and the dilution effect of water (coming from ATH decomposition) is smaller. As a consequence, the fuel consists of more flammable gases than it is the case for EVM-ATH. Concentration of released water is not high enough to dilute the fuel sufficiently to prevent ignition. When material ignites, the concentrations of acetic acid and ammonia decrease abruptly due to the fact that they are burning. After ignition, nitrogen oxide is detected (not presented in Fig. 10) due to combustion of ammonia. A maximum quantity of nitrogen oxide of 59 ppm is detected just after ignition; afterwards the concentration decreases constantly until flameout. In total, 1460 ppm of nitrogen oxide are released. Nitrogen dioxide was not detected in the gas phase which is explained by the combustion reaction of ammonia [25]:

$$2\,NH_3 + 4\,O_2 \rightarrow 2\,NO + 3\,H_2O$$

Moreover, after ignition, concentration of water and carbon dioxide increases sharply due to complete combustion of the material. Both gases reach maximum concentration before $pHRR_1$: 6543 ppm in the case of water and 12261 ppm for carbon dioxide. Afterwards concentrations decrease constantly until the end of the experiment. The concentration of carbon monoxide, indicating incomplete combustion, increases constantly from the ignition of the material until the flameout. At the flame out, a maximum of 565 ppm release is observed at the flame out; then concentration of carbon monoxide decreases until end of experiment.

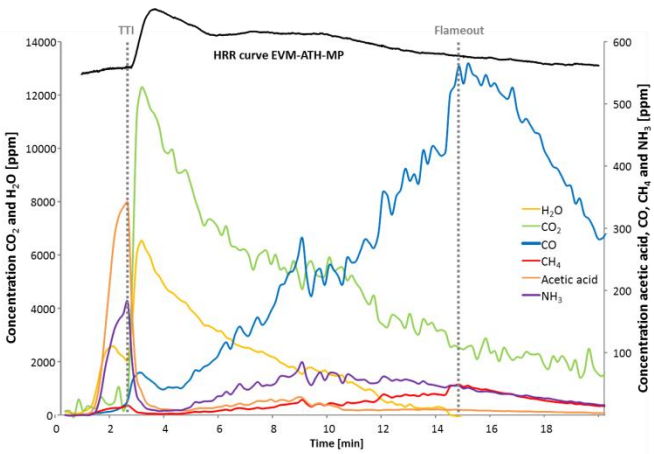

Fig. 12: Spectra obtained by MLC-FTIR for EVM-ATH-MP

Table 4: Quantification of released gases during MLC-FTIR experiment for EVM-ATH

Gas	Total quantity released [ppm]	Released before ignition [ppm]	Released before ignition [%]
H_2O	169 302	17 830	11
CO_2	517 772	5 912	1
CO	30 477	74	0
CH_4	2 259	87	4
NH_3	5 104	867	17
HCN	632	6	1
NO	1460	40	3
Acetic acid	3 126	1 738	56

Concerning release of acetic acid, ammonia and methane, it can be seen that the three gases show the same profile after ignition: After ignition concentration decreased until $pHRR_1$. Then, concentrations increase until $pHRR_2$. Afterwards concentration decreases until the end of experiment. The increase of concentration of acetic acid, ammonia and methane before $pHRR_2$ suggests that a protective layer is formed at the

RSC Advances Accepted Manuscript

beginning of the experiment which cracks after $pHRR_1$ and releases gases trapped under the layer formed before (as for EVM-ATH). Whereas it can be clearly seen that increase of gas concentration is significantly lower than for EVM-ATH. It can therefore be assumed that the protective layer formed at the material surface is more stable and accordingly more effective in the case of EVM-ATH-MP than it is the case for EVM-ATH. A more effective protective layer explains reduced $pHRR_2$ for EVM-ATH-MP.

Regarding the total quantities of gases released during experiment it appears that in the case of EVM-ATH-MP, 30604 ppm of carbon monoxide is evolved during combustion process which is nearly two times higher than in the case of EVM-ATH (18368 ppm). It is concluded that incomplete combustion is more likely when MP is present in the material. An evidence for the presence of acetone in the gas phase during MLC-FTIR experiment was not found.

As a short conclusion for the analysis of the gas phase of EVM-ATH-MP (py-GCMS, MLC-FTIR), it can be said that the material is protected through endothermic decomposition of ATH and the resulting release of water. However, presence of MP leads to earlier ignition due to ammonia released from MP decomposition. Moreover, presence of MP leads to higher release of carbon monoxide than it is the case for EVM-ATH. Concerning gases released during thermo-oxidative and pyrolytic decomposition, it was found that the polymer degrades following the pathway described for EVM-ATH: deacetylation of the polymer forming polyenes which are then degraded. At low heating rates saturated and mono unsaturated linear hydrocarbons are formed; high heating ramps lead to favoured formation of benzene and its homologues.

3.3.3 Condensed phase analysis

The condensed phase was analysed using a method in which the combustion process is stopped at characteristic times during the cone calorimeter experiment. Samples were removed from the external heat source and flames were quenched immediately to prevent further decomposition. The resulting materials afterwards were analysed by solid state NMR (^{13}P, ^{13}C and ^{27}Al). The top of the resting plates, i.e. the char and the bottom, i.e. the protected plate under the char were analysed separately.

EVM-ATH

For EVM-ATH the combustion was stopped at six characteristic points: before the ignition (230 s), during increase (245 s), at the $pHRR_1$ (275 s), at the $pHRR_2$ (444 s), during decrease (700 s) and at the end of combustion (1200 s). The residues (Fig. 13) were analysed by ^{13}C and ^{27}Al solid state NMR.

^{13}C spectra obtained at the different stages of combustion are presented in Fig. 14. The spectrum of the unburned material (a) shows several peaks (attribution of observed chemical shifts presented in Table 5). The spectrum corresponds to data reported already in literature for pure EVM [17, 26-30]. The peak at 20.8 ppm corresponds to CH_3-group of the acetic acid functionality of the polymer [28]. Those at 25.1, 29.8 and 34.5 ppm are attributed to CH_2–groups in the polymer backbone [27, 31]. The multiplicity of the peaks is due to the fact that when VA monomer copolymerizes with ethylene, a random copolymer is obtained leading to several different monomer sequences in the chain. According to Delfini et al. [32], the chemical shift depends on the position of the carbon in a monomer.

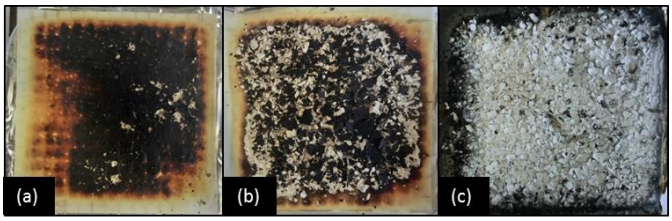

Fig 13: Residues of EVM-ATH (a) after ignition (b) at $pHRR_1$ (c) at end of combustion

However, this work was carried out in liquid state NMR, and thus does not take into account structural effects, but, since all the reported bands are present on our solid state NMR spectrum, it can be assumed that the assignments are transposable. Peaks assigned to CH are detected around 70 ppm. The multiplicity of the CH chemical shift is also explained by the sequence distribution of pentads in the polymer [32].

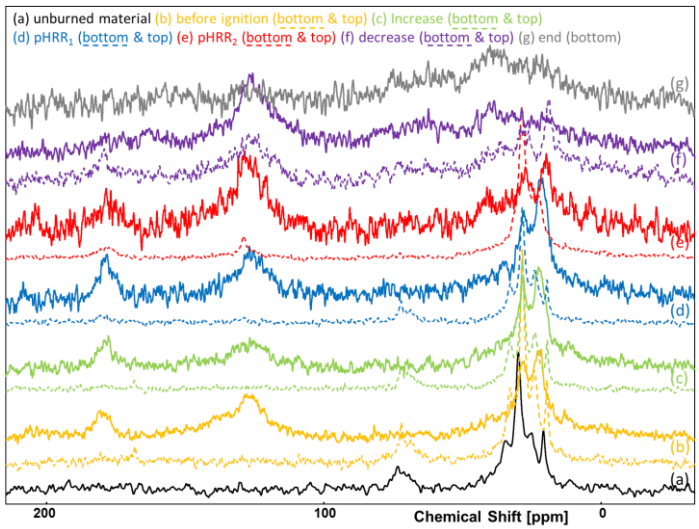

Fig 14: ^{13}C spectra obtained for different stages of combustion of EVM-ATH

Table 5: Attribution of chemical shifts obtained for EVM-ATH and EVM-ATH-MP

Chemical Shift [ppm]	Attribution
20.8	CH_3
25.1, 29.8, 34.5 and ~ 42	CH_2
69.3, 71.2 and 73.4, 76.1	CH
129.5	Unsaturated hydrocarbons
169.4	C=O in acetate/C=N in melamine
182.0, 180.9, 180 and 178.7	C=O (carbonyl)

The chemical shift at 170 ppm corresponding to C=O in the acetate group is not observed for the pure polymer. Due to the fact that this peak is obtained for the pure polymer (Fig. 15) it can be said that the absence of the C=O peak in unburnt EVM-

RSC Advances Accepted Manuscript

This journal is © The Royal Society of Chemistry 2014

ATH is due to the large anisotropy of the chemical shift tensor of C=O [33].

The spectra of samples taken before ignition of the materials show changes in comparison to the pure polymer. The sample taken at the bottom of the plate exhibits an additional peak at 169 ppm. This peak is assigned to C=O in the carbonyl function in acetic acid. The spectrum of the top of the sample taken before ignition shows a peak corresponding to aliphatic hydrocarbons. Additionally, a broad peak around 130 ppm, appears signalizing the formation of unsaturated hydrocarbon structures (char). Moreover, a multiple peak around 180 ppm (182.0, 180.9, 180.0 and 178.7 ppm) is observed in the residue taken before the ignition (top of plate). This peak is attributed to carbonyl (C=O) indicating that oxidized unsaturated hydrocarbons are present in the residue.

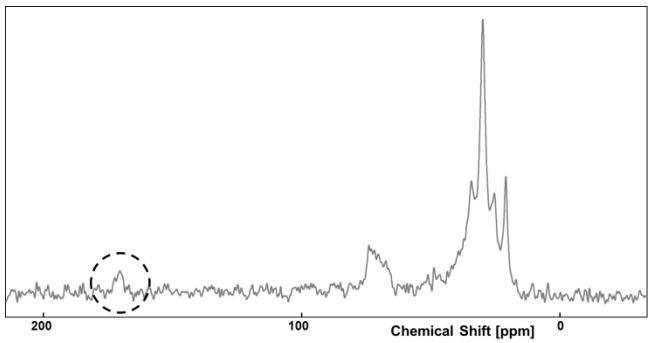

Fig 15: ^{13}C spectra obtained for unburnt EVM

Spectra recorded after ignition, at the increase of the curve (top and bottom) are identical to those obtained before the ignition. At the $pHRR_1$, the spectrum recorded for the bottom of the plate is similar to that obtained before the ignition at the bottom. This observation indicates that the material under the char layer is still protected. At the top of the plate and at the $pHRR_1$ a change of the spectra in comparison to before ignition is observed: the chemical shift attributed to methyl of acetic acid group has disappeared. It can therefore be said that at the top of the plate the deacetylation process of the polymer is completed. Nevertheless, peaks around 180 ppm indicate that molecules containing carbonyls are still present in the condensed phase. At the $pHRR_2$, the spectrum of the residue taken at the bottom of the plate changes. Peaks corresponding to CH_2 (29.6 and 24.8 ppm), unsaturated hydrocarbons (130 ppm) and carbonyls (180 ppm) are observed. At the $pHRR_2$, the deacetylation of the polymer is completed in the whole material and saturated and unsaturated hydrocarbons are present in the residue. At the same time the broad peak corresponding to carbonyl functions indicating presence of oxidation of the char structure is still present. The top of the plate at the $pHRR_2$, as well as the bottom of the plate at the decrease show exactly the same chemical shifts as described for the bottom of the plate taken at $pHRR_2$. The top of the plate taken at the decrease only shows chemical shifts assigned to saturated (CH_2) and unsaturated hydrocarbons. At the end of the combustion only the spectrum of the bottom of the sample was recorded. The top of the residue did not show any results even after accumulation of the spectra for a longer time. The reduction of the resolution of the ^{13}C signal is related to the anisotropy of the paramagnetic susceptibility of the aromatic compounds present in the residue. In the case of paramagnetic materials, this anisotropy is large and, consequently, leads to disappearance of the ^{13}C signal.

^{27}Al spectra of the residues of EVM-ATH are presented in Fig 16. The unburnt material exhibits a peak at 8 ppm corresponding to octahedral coordinated aluminium [34]. An additional site is observed at -2.9 ppm. The recorded spectrum corresponds to the spectrum for gibbsite ($Al(OH)_3$) found in literature [35, 36]. In gibbsite hydroxyl ions are hexagonal close packed with aluminium ions in octahedral co-ordination. The bottom of the sample taken before ignition of the material has the same spectrum like the unburnt material. The spectrum recorded at the top of the plate shows an additional chemical shift at 65.0 ppm attributed to tetrahedral coordinated aluminium.

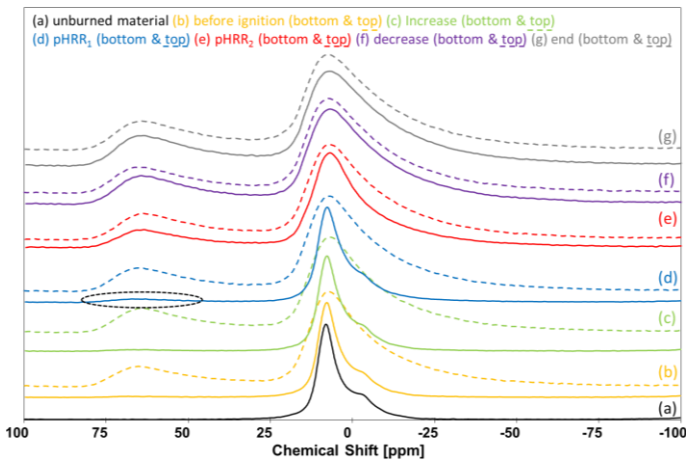

Fig 16: ^{27}Al spectra obtained for different stages of combustion of EVM-ATH

The appearance of this peak indicates the thermal decomposition of ATH releasing water and leading to the formation of alumina consisting of a close packed oxygen lattice where Al^{3+} occupies tetrahedral and octahedral holes. The ratio of AlO_4 to AlO_6 (simulated using Dmfit [37]) is 1:4. As mentioned during analysis of the thermal decomposition of ATH, it is known that ATH (gibbsite form) degrades forming alumina (Al_2O_3). It is known that boehmite and corundum consist of only octahedral coordinated Al-ions, whereas several crystal structures of alumina are possible[35, 36]. The most commonly form of alumina is α-alumina which consists of only octahedral coordinated Al-ions. The same is true for boehmite, formed during dehydration of gibbsite, only octahedral coordinated Al-ions are present. Due to the fact that in our case tetrahedral and octahedral coordinated Al-ions are present in the condensed phase it can be concluded that also η- or θ-alumina (consisting of both tetrahedral and octahedral sites) is formed. Nevertheless it can be said that the alumina consisting of only octahedral coordinated Al-ions, i.e. boehmite and alumina, are mainly formed due to the ratio of AlO_4 to AlO_6 of

RSC Advances Accepted Manuscript

1:4. Moreover, it can be seen that the peak corresponding to octahedral coordinated Al is getting broader with progressed combustion time. Widening of the peak is explained by decreasing of crystallinity of the formed product. Regarding the spectra recorded for the other stages of combustion it can be seen, that the bottom of the sample taken at the increase exhibits the same spectra as the unburnt material. This observation shows that the underlying material is still protected and that not all of ATH present in the material is degraded. First change of the spectrum of the underlying material is obtained at the $pHRR_1$, where a small peak corresponding to tetrahedral coordinated Al is found (ratio AlO_4/AlO_6 = 7/100). It can therefore be concluded that only a small part of ATH is degraded at this stage of the combustion. Concerning top of the samples taken at the different stages of combustion it can be seen that all spectra exhibit the same chemical shifts, corresponding to tetrahedral and octahedral coordinated Al-ions. Moreover the ratio AlO_4/AlO_6 is the same for all other samples (1:4).

It has further to be noted that water detected after ignition of EVM-ATH during MLC-FTIR experiment, is not only due to complete combustion but also to the dehydration of ATH occurring until the $pHRR_1$. Presence of a char protecting the material at its surface can be evidenced through the fact that ^{27}Al NMR showed that ATH is not fully degraded until $pHRR_1$, the underlying material is protected through a layer formed at the sample surface consisting of alumina and saturated and unsaturated hydrocarbons. This result is different to the results found in earlier studies [38]. In this study, an ethylene vinyl acetate polymer having a VA content of 24 % is studied. It is shown that when 65 wt% ATH are incorporated into the polymeric matrix, ATH is completely degraded into alumina oxide before ignition of the material. The difference between the results found in this study and in our actual study is explained by the different conditions used. First, the VA content of the polymer in our study is much higher. Secondly, residues were obtained stopping MLC experiment carried at 50 kW/m², whereas 35 kW/m² is used in our case.

EVM-ATH-MP

Combustion of EVM-ATH-MP was stopped at six characteristic points: before the ignition (120 s), during increase (175 s), at the $pHRR_1$ (190 s), at the $pHRR_2$ (425 s), during decrease (700 s) and at the end of combustion (1200 s). Residues (Fig. 17) were analysed by ^{13}C, ^{27}Al and ^{31}P solid state NMR.

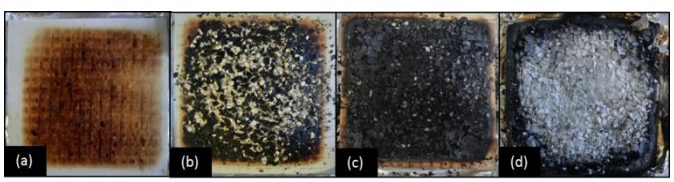

Fig 17: Residues of EVM-ATH-MP (a) after ignition (b) at $pHRR_1$ (c) at $pHRR_2$ (d) at end of combustion

^{13}C NMR spectra of the residues at different stages of combustion are presented in Fig. 18. The unburnt material exhibits the same chemical shift as unburnt EVM-ATH. Peaks attributed to CH_3 (20.8 ppm), CH_2 (25.5, 29.8 and 33.9 ppm), and CH (73.4 ppm) are observed. Additionally, two peaks at 157.3 and 165. 4 ppm attributed to MP (melamine ring) are present [39, 40]. These chemical shifts could also be due to the quaternary C atom connecting the vinyl acetate groups to the polymer backbone. Nevertheless, this possibility is excluded due to the fact that the peak is not present in unburnt EVM-ATH.

Before ignition of the material, at the bottom of the plate, only the chemical shift at 157 ppm is present. It is known that condensation products of melamine exhibit chemical shifts around 156 and 164 ppm. Due to the fact that the peak corresponding to MP is not shifted to these resonances it is concluded that melamine is present in its non-condensed form. Moreover a peak at 180 ppm corresponding to carbonyl structures (C=O) in carboxylic acids is observed. Peaks corresponding to CH, CH_2 and CH_3 are still present. At the top of the plate taken before ignition, the intensity of the peak corresponding to the methyl group of vinyl acetate decreases and additional peaks at 130 ppm (unsaturated hydrocarbons) and 180 ppm (carbonyl) are observed. These peaks indicate the presence of an oxidized, aromatic char. The spectrum of the bottom of the sample taken at the increase is equal to the one obtained before ignition (bottom). The top of the plate at this stage of the combustion process exhibits chemical shifts corresponding to CH_2-groups, unsaturated hydrocarbons (130 ppm) and 182.1 ppm corresponding to carbonyl functions. A peak at 167 ppm attributed to melamine [40] can be suspected whereas its intensity is very low. At the same time, this chemical shift can also be attributed to the carbonyl function present in the acetate group of the polymer.

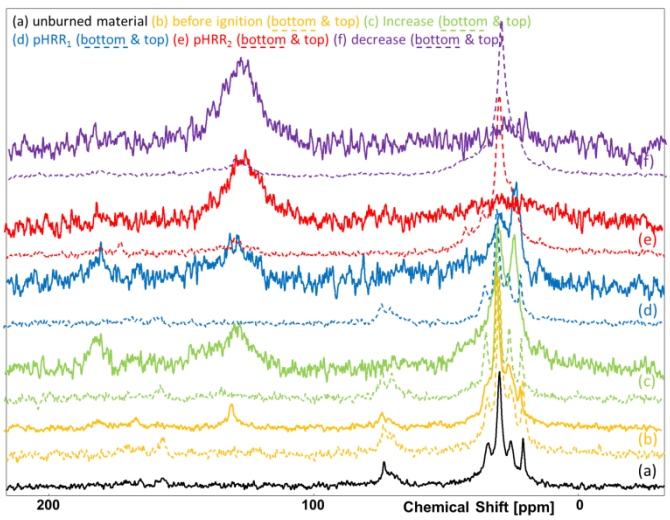

Fig 18: ^{13}C spectra obtained for different stages of combustion of EVM-ATH-MP

At $pHRR_1$, the spectrum of the bottom of the plate is similar to that obtained at the increase which indicates that the bulk material under the protective layer is protected until the $pHRR_1$. Peaks corresponding to methyl in the vinyl acetate group are

RSC Advances Accepted Manuscript

This journal is © The Royal Society of Chemistry 2014

still present. For the top of the plate taken at the $pHRR_1$, peaks corresponding to CH_2-groups (23.3 and 29.6 ppm), unsaturated hydrocarbons (130 ppm) and carbonyl functions (180 ppm) are observed.

Spectra of the bottom of the plate at the $pHRR_2$ consists of chemical shifts corresponding to CH_2-groups (29.8 ppm) and unsaturated hydrocarbon structures (130 ppm) as well as a chemical shift assigned to carbonyl functions (oxidation of the char) are obtained (180 ppm). The residues of the top of the plate taken at $pHHR_2$ only exhibit chemical shift at 130 ppm indicating the presence of unsaturated hydrocarbon structures (charring peak). The same is true for the spectrum taken of the top of the plate at the decrease. The bottom of the plate at the decrease shows the same peaks as the spectrum taken at the bottom of $pHRR_2$ whereas the peak corresponding to carbonyl is found at 181 ppm. Spectra of the residues left at the end of the experiment give no signal due to low content (or possible absence) of carbon atoms in the residues. Reduction of the resolution of the ^{13}C signal is due to increased anisotropy of paramagnetic susceptibility of carbon atoms present in the residue.

^{27}Al NMR spectra of the residues are presented in Fig. 19. The spectrum obtained for unburnt EVM-ATH-MP is similar to that obtained for unburnt EVM-ATH. The chemical shift at 7.9 ppm with a small shoulder at -2.0 ppm is attributed to octahedral coordinated Al^{3+} [34].

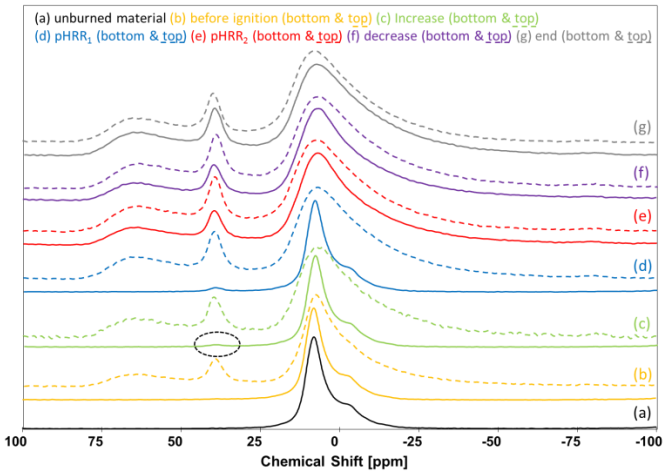

Fig 19: ^{27}Al spectra obtained for different stages of combustion of EVM-ATH-MP

At the top of the plate taken before the ignition a peak assigned to tetrahedral coordination of aluminium indicating the dehydration of ATH forming an aluminium oxide is detected (65 ppm). The underlying material (bottom of the plates) has the same spectra like unburnt EVM-ATH-MP until $pHRR_1$. Top of the plates always show chemical shifts corresponding to tetrahedral and octahedral coordinated aluminium. As for EVM-ATH, the peak corresponding to octahedral coordinated Al is getting broader with progressed combustion process. It is assumed that a char layer consisting of unsaturated hydrocarbons and aluminium oxide is formed protecting the material against heat. This indicates that decomposition of ATH is completed after $pHRR_1$. Hence the material is protected through endothermic dehydration of ATH and the resulting release of water until $pHRR_1$.

Moreover, an additional peak is observed at around 39.5 ppm assigned to aluminium phosphate (AlO_4), whereas Al^{3+} has a tetrahedral coordination (AlO_4) [41, 42]. This peak is observed in all spectra of samples taken at the top of the plates. Concerning the bottom of the plates, $AlPO_4$ is observed for the first time at the increase.

It can be seen that phosphate present in MP coordinates with Al present in the condensed phase to form aluminium phosphate when melamine is evolved due to decomposition of MP (corresponds to ^{13}C NMR results of EVM-ATH-MP). The peak assigned to aluminium phosphate is present in all residues taken at the top of samples for each step of the combustion process. Bourbigot et al. [33] showed that formation of orthophosphates in intumescent systems improves stability the protective layer. They proposed that formed char layer consisting of aromatic and aliphatic molecules is bridged by the phosphates leading to improved properties of the protective char layer. These results are in agreement with those found in this study. During MLC experiment, it was found that $pHRR_2$ is lower for EVM-ATH-MP than it is for EVM-ATH. It is therefore supposed that formation of aluminium phosphate during decomposition of EVM-ATH-MP leads to formation of a protective layer at the material surface exhibiting higher insulative properties. It is assumed that phosphates formed during decomposition of EVM-ATH-MP bridge the aromatic char system developed during combustion to form a more stable protective char layer. The formation of aluminium phosphate improving the efficiency of the char layer supports the assumption postulated in discussion of MLC-FTIR results. It was supposed that the gas flow at $pHRR_2$ is lower for EVM-ATH-MP due to formation of a more insulative protective layer.

The formation of aluminium phosphate is confirmed by analysis of the residues by ^{31}P NMR (Fig. 20). It can be seen that the peak corresponding to aluminium phosphate (-30 ppm) is observed in all samples taken at the bottom of the plate and in samples taken at the bottom from the increase to the end of the combustion. The unburnt material exhibits a peak at 1.3 ppm having a shoulder at -1 ppm corresponding to orthophosphate. The presence of these two peaks indicates different structures of the orthophosphates. The orthophosphate species have either one or two neighbour aluminium atoms . It can be seen that the chemical shift corresponding to orthophosphate changes a little bit before ignition of the material (bottom of the plate): the shoulder at -1 ppm is getting more important than the signal at 1.3 ppm. This change is explained through structure changes taking place due to decomposition of MP which is known to evolve melamine.

All together it can be said that the phosphate present in MP is degraded to $AlPO_4$ during decomposition. It is supposed that this compound has a role in the formation of a protective surface layer which protects the material against the attack of fire and improved properties of this layer.

RSC Advances Accepted Manuscript

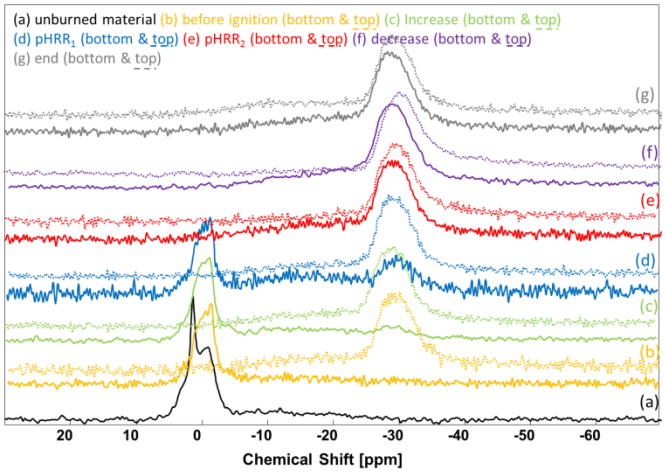

Fig 20: ^{31}P spectra obtained for different stages of combustion of EVM-ATH-MP

Protection mechanism for the EVM-ATH and EVM-ATH-MP

It was found that EVM-ATH is protected through a gas phase and a condensed phase mechanism. In the condensed phase, ATH degrades forming alumina. Decomposition of the polymer results in formation of a protective layer. The developped layer protects the material against the attack of fire. At the same time, water coming from the dehydration of ATH dilutes the fuel and prevents early igniton reinforced by the endothermic dehydration of ATH. Concerning decomposition of the polymer, it was found that deacetylation of EVM evolving acetic acid takes place before ignition. Linear polyenes formed during deacetylation are degraded afterwards whereas the nature of released gases depends on the heating rate. Low heating rates lead to formation of linear saturated and mono unsaturated hydrocarbons whereas high heating rates lead to formation to benzene and its homologues and small linear unsaturated hydrocarbons (mono and di unsaturated). In the case of EVM-ATH-MP, ATH exhibits the same action in the gas phase and in the condensed phase as it was found for EVM-ATH. Analysis of the role of MP in the system showed that release of ammonia (from MP decomposition) leads to earlier ignition of the material. At the same time, phosphates remaining in the condensed phase after decomposition of MP form aluminum phosphates. The formed aluminum phosphates connected aliphatic and aromatic molecules which are present in the protective layer at the material surface. The protective layer of EVM-ATH-MP improves the barrier effect of the protective layer. Due to improved efficiency of the char layer, release of heat, decomposition gases and smoke in the second part of the combustion process is reduced in comparison to EVM-ATH.

Conclusions

Flame retardant properties and smoke release of EVM materials were investigated using ATH and MP as fire retardant additives. It was found that partial replacement of ATH by MP leads to earlier ignition of the material and reduction of $pHRR_2$. To understand the role of MP in the system both materials, i.e. EVM-ATH and EVM-ATH-MP were further analysed. It was found that all additives are well dispersed in the polymeric matrix. Decomposition mechanism of both materials was investigated. It was detected that both materials are protected by a gas phase mechanism: decomposition of ATH evolves water diluting the fuel. At the same time ATH has a cooling effect due to its endothermic decomposition. Early ignition of EVM-ATH-MP was explained by presence of more flammable gases, i.e. ammonia, coming from decomposition of MP. It was also found that structure of released gases depend on the used heating ramp. Condensed phase mechanism was analysed for both materials: a physical barrier is formed during combustion protecting the material against external heat. The presence of MP leads formation of aluminium phosphate in the condensed phase improving stability and insulative properties of the char layer.

Acknowledgements

The authors want to thank Séverine Bellayer for her help with SEM images. Further they thank Betrand Revel and Betrand Doumert for their support performing NMR spectra.

Notes and references

[a] R_2Fire group/UMET – UMR CNRS 8207, Ecole Nationale Supérieure de Chimie de Lille (ENSCL), University of Lille, 59652 Villeneuve d'Ascq, France
[b] LANXESS Deutschland GmbH, 50569 Köln, Germany

1. Overall Fire Death Rates and Relative Risk (2001-2010), http://www.usfa.fema.gov/statistics/estimates/trend_overall.shtm, 2013.
2. G. Camino, A. Maffezzoli, M. Braglia, L. M. De and M. Zammarano, *Polymer Degradadation and Stability*, 2001, **74**, 457-464.
3. X. Zhang, F. Guo, J. Chen, G. Wang and H. Liu, *Polymer Degradation and Stability*, 2005, **87**, 411-418.
4. A. A. Basfar and H. J. Bae, *Journal of Fire Sciences*, 2010, **28**, 161-180.
5. C. Jiao, Z. Wang, X. Chen, B. Yu and Y. Hu, *Radiation Physics and Chemistry*, 2006, **75**, 557-563.
6. A. Riva, G. Camino, L. Fomperie and P. Amigouët, *Polymer Degradation and Stability*, 2003, **82**, 341-346.
7. L. Du, B. Qu and Z. Xu, *Polymer Degradation and Stability*, 2006, **91**, 995-1001.
8. J. Zilberman, T. R. Hull, D. Price, G. J. Milnes and F. Keen, *Fire and Materials*, 2000, **24**, 159-164.
9. M. Fu and B. Qu, *Polymer Degradation and Stability*, 2004, **85**, 633-639.
10. L. Ye, Y. Miao, H. Yan, Z. Li, Y. Zhou, J. Liu and H. Liu, *Polymer Degradation and Stability*, 2013, **98**, 868-874.
11. L. Clerc, L. Ferry, E. Leroy and J.-M. Lopez-Cuesta, *Polymer Degradation and Stability*, 2005, **88**, 504-511.
12. F. Laoutid, P. Gaudon, J. M. Taulemesse, J. M. Lopez Cuesta, J. I. Velasco and A. Piechaczyk, *Polymer Degradation and Stability*, 2006, **91**, 3074-3082.
13. A. Szép, A. Szabó, N. Tóth, P. Anna and G. Marosi, *Polymer Degradation and Stability*, 2006, **91**, 593-599.
14. A. Ahamad, C. B. Patil, P. P. Mahulikar, D. G. Hundiwale and V. V. Gite, *Journal of Elastomers and Plastics*, 2012, **44**, 251-261.

RSC Advances Accepted Manuscript

 This journal is © The Royal Society of Chemistry 2014

15. Y.-Y. Yen, H.-T. Wang and W.-J. Guo, *Polymer Degradation and Stability*, 2012, **97**, 863-869.
16. L. Ye, Q. Wu and B. Qu, *Polymer Degradation and Stability*, 2009, **94**, 751-756.
17. O. Cérin, S. Duquesne, G. Fontaine, A. Roos and S. Bourbigot, *Polymer Degradation and Stability*, 2011, **96**, 1812-1820.
18. O. Cérin, University of Lille 1 - Sciences and Technologies, France, 2010.
19. W. Xing, L. Song, H. Lu, Y. Hu and S. Zhou, *Polymers for Advanced Technologies*, 2009, **20**, 696-702.
20. Z. Wang, P. Lv, Y. Hu and K. Hu, *Journal of Analytical and Applied Pyrolysis*, 2009, **86**, 207-214.
21. S. Zhou, Z. Wang, Z. Gui and Y. Hu, *Fire and Materials*, 2008, **32**, 307-319.
22. L. Costa, G. Camino and d. C. M. P. Luda, *ACS Symp. Ser.*, 1990, **425**, 211-238.
23. A. Witkowski, A. A. Stec and T. Richard Hull, *Polymer Degradation and Stability*, 2012, **97**, 2231-2240.
24. F. E. Ngohang, G. Fontaine, L. Gay and S. Bourbigot, *Polymer Degradation and Stability*, 2014, **in press**.
25. J. F. Grcar, P. Glarborg, J. B. Bell, M. S. Day, A. Loren and A. D. Jensen, *Proceedings of the Combustion Institute*, 2005, **30**, 1193-1200.
26. J. L. MacDonald, U. Werner-Zwanziger, B. Chen, J. W. Zwanziger and D. Forgeron, *Solid State Nucl. Magn. Reson.*, 2011, **40**, 78-83.
27. G. C. Stael and M. I. B. Tavares, *Polymer Testing*, 1997, **16**, 193-198.
28. N. Pécoul, S. Bourbigot and B. Revel, *Macromolecular Symposia*, 1997, **119**, 309-315.
29. J. Rottstegge, M. Arnold, L. Herschke, G. Glasser, M. Wilhelm, H. W. Spiess and W. D. Hergeth, *Cem. Concr. Res.*, 2005, **35**, 2233-2243.
30. C. M. G. de Souza and M. I. B. Tavares, *Polym. Test.*, 1998, **17**, 533-541.
31. F. Carpentier, S. Bourbigot, M. Le Bras, R. Delobel and M. Foulon, *Polym. Degrad. Stab.*, 2000, **69**, 83-92.
32. M. Delfini, A. L. Segre and F. Conti, *Macromolecules*, 1973, **6**, 456-459.
33. S. Bourbigot, M. L. Bras and R. Delobel, *Carbon*, 1993, **31**, 1219-1230.
34. J. Sanz and J. M. Serratosa, *Clay Minerals*, 1984, **19**, 113-115.
35. R. C. T. Slade, J. C. Southern and I. M. Thompson, *Journal of Materials Chemistry*, 1991, **1**, 563-568.
36. V. J. Ingram-Jones, R. C. T. Slade, T. W. Davies, J. C. Southern and S. Salvador, *Journal of Materials Chemistry*, 1996, **6**, 73-79.
37. D. Massiot, Dmfit, 2011.
38. S. Bourbigot, M. L. Bras, R. Leeuwendal, K. K. Shen and D. Schubert, *Polymer Degradation and Stability*, 1999, **64**, 419-425.
39. S. Jahromi, W. Gabriëlse and A. Braam, *Polymer*, 2003, **44**, 25-37.
40. P. Ducrocq, S. Duquesne, S. Magnet, S. Bourbigot and R. Delobel, *Progress in Organic Coatings*, 2006, **57**, 430-438.
41. R. J. Kirkpatrick and R. K. Brow, *Solid State Nuclear Magnetic Resonance*, 1995, **5**, 9-21.
42. J. Quartararo, M. Guelton, M. Rigole, J.-P. Amoureux, C. Fernandez and J. Grimblot, *Journal of Materials Chemistry*, 1999, **9**, 2637-2646.

RSC Advances Accepted Manuscript